Supporting Information

Roelants et al. 10.1073/pnas.1100633108

SI Methods

An overview of the methods is provided as a flowchart in Fig. S1.

Morphological Dataset. The matrix published by Haas (1) includes 136 larval characters for 81 ingroup taxa representing the major anuran lineages and covering a broad morphological and ecological diversity (Fig. S1, 1). Our analyses are restricted to free-living tadpoles, and it is likely that some taxa not included here might occupy additional regions of morphospace (direct developing taxa in particular). However, it is improbable that their addition would drastically alter our conclusions about patterns and rates of evolution across subsequent radiations. Four salamanders were added as an outgroup, two of which (*Pleurodeles waltl* and *Lissotriton alpestris*) showed identical states for all characters. We excluded five characters, because they were either continuous [characters 12, 83, 116, and 117 by Haas (1)] or ontogenetically ambiguous (character 102). The remaining 131 characters cover major tissue types and body parts. We defined the following characters subsets to investigate patterns of evolutionary rates and homoplasy (numbers corresponding to ref. 1):

Characters defining the tadpole morphotypes by Orton (1–5): 3, 4, 6–8, 16–18, 28, 71, 74, 84, 92, 124, 128–130, 132, and 136.
Connective tissue characters: 66–82, 84–92, 94–101, 103–115, 118–120, 122, 123, and 125–127.
Epithelial tissue characters: 1–9, 13–18, 121, 124, 128–131, and 133–136.
Muscular tissue characters: 19–62.
Axial characters: 14, 15, 99, 100, 101, 121, 132, and 133.
Branchial characters: 19–22, 24–41, 103–115, 118–120, and 134–136.
Cranial characters: 11, 42–47, 52–82, 96–98, 122, and 131.
Opercular characters: 16–18, 23, 123, and 124.
Oral/jaw characters: 3–10, 48–51, 84–95, and 125–130.

Construction of a Molecular Scaffold Tree. To obtain a robust phylogenetic scaffold tree that overlapped maximally in taxon sampling with the morphological dataset (Fig. S1, 2 and 3), we used a four-step approach.

i) We retrieved GenBank sequence data for 164 amphibian species that were identical or presumed to be closely related (mostly congeneric and sometimes confamilial) to those in the morphological dataset, were useful in breaking up long branches in the anuran tree (*Caudiverbera*, *Leiopelma*, and *Myobatrachus*), or assisted in rooting the tree (the caecilians *Hypogeophis*, *Ichthyophis*, and *Rhinatrema*) (Dataset S1). Obtained sequences encompassed a mitochondrial segment spanning 12S rRNA (partially), $tRNA^{Val}$, 16S rRNA, $tRNA^{Leu}$, and ND-1 (partially) and 12 nuclear gene fragments (BDNF, c-Myc, CXCR-4, Histone H3a, Ncx-1, POMCA, RAG-1, RAG-2, Rhodopsin, SIA, Slc8a-3, and Tyrosinase). Alignments for all fragments were created with ClustalX 1.81 (6) and concatenated to obtain a single multigene matrix. Ambiguously aligned positions in the periphery of indels were excluded from further analysis, which resulted in a matrix of 11,204 bp.

ii) The 164-taxon dataset was submitted to 500 replicates of rapid bootstrapping (RBS) (7) under the likelihood criterion using RAxML 7.0.4 (8) to ensure close relationships between congeneric and confamilial species. High RBS values (>75%) confirmed this in all cases (Fig. S2) except for *Nyctimystes*, where *N. dayi* was found to be more closely related to Australian *Litoria* species than to Papuan *Nyctimystes* species. Complementary sequences of confirmed closely related species were combined into single chimeric taxa to maximize the amount of aligned positions per taxon. This resulted in a matrix of 84 chimeric taxa, including 78 anurans (75 taxa for which morphological data are available and 3 taxa that assist in breaking up long branches), 3 caudates, and 3 caecilians (Dataset S1).

iii) The 84-taxon dataset was used to assess anuran clade support by 1,000 replicates of standard bootstrapping (SBS) using RaxML and by Bayesian posterior probabilities (BPP) using MrBayes 3.2.1 (9). Both methods implemented a mixed general time-reversible model (GTR + G + I) partitioned over the different gene fragments (12SrRNA, 16SrRNA, and two tRNA genes were treated as a single noncoding partition subset). The SBS analyses were performed with empirical base frequencies; remaining model parameters were optimized per partition subset. The Bayesian analyses implemented flat dirichlet priors for base frequencies and substitution rate matrices and uniform priors for among-site rate parameters. Two parallel Markov chain Monte Carlo (MCMC) runs of four incrementally heated (temperature parameter = 0.2) chains were performed, with a length of 10,000,000 generations, a sampling frequency of 1 per 2,000 generations, and a burn-in corresponding to the first 2,000,000 generations. Convergence of the parallel runs was confirmed by split frequency SDs (<0.01) and potential scale reduction factors (~1.0) for all model parameters, as reported by MrBayes. Adequate posterior sampling was checked by verifying with Tracer 1.4 (10) if the runs had reached effective sampling sizes >200 for all model parameters.

iv) The scaffold tree was built by incorporating nodes that received high statistical support by our clade support analyses (SBS > 75% and/or BPP > 0.95) and received high support or were consistently recovered in previously published studies (Fig. S3) (11–43). As a consequence, the resulting scaffold tree is highly consistent with most molecular phylogenetic analyses conducted so far.

Morphological Analyses. ***Phylogeny inference.*** The molecular scaffold tree was used to constrain heuristic maximum parsimony (MP) and Bayesian analyses of the morphological dataset performed with PAUP* 4.0b10 (44) and MrBayes, respectively (Fig. S1, 4). Similar strategies of analyzing morphological data with topological constraints derived from molecular data have been used before (45, 46). Heuristic MP searches involved 1,000 replicates of random taxon addition, tree bissecton-reconnection (TBR) branch swapping, and Multrees option switched off to allow efficient exploration of multiple tree islands. The MP trees retained from multiple islands were subsequently used as starting trees for additional rounds of TBR branch swapping with the Multrees option activated to explore individual islands more thoroughly. All characters were equally weighted, multistate character scores were treated as polymorphisms, and 13 characters were treated as ordered (using ref. 1). The molecular scaffold tree was implemented as a backbone constraint, leaving the freedom for full optimization of the phylogenetic position of the six taxa that were represented in the morphological dataset but not in the scaffold tree (*Bombina maxima*, *Bufo brongersmai*, *L. inermis*, *L. rheocola*, *Peltophryne peltocephala*, and *Phyllomedusa distincta*). The analyses yielded 1,760 equally parsimonious MP trees (tree length = 652; consistency index = 0.2914; retention index = 0.7240), which, because of the imposed

constraints, differed mainly in the basal nodes within the microhylid and nobleobatrachian radiations.

Precompiled versions of MrBayes 3.1.2 allow a default maximum of 30 nodal constraints, and therefore, to incorporate the entire molecular scaffold, the source code of MrBayes had to be modified and recompiled. Because MrBayes does not allow the implementation of backbone constraints, we excluded the six taxa absent in the scaffold tree. We applied an Mk1 model of discrete character change (47) with default prior settings for all parameters and γ-correction for rate heterogeneity among characters (i.e., a Mk1 + G model). Comparison of likelihood scores of posteriorly sampled trees obtained under this model indicated a much better fit to the data than a plain Mk1 model (analogy with most molecular datasets, where correction of rate heterogeneity represents a dramatic model improvement) (48). The MCMC chains were run for 5 million generations, with a sampling frequency of 1 per 1,000 and a burn-in corresponding to the first 1 million generations. All other settings, as well as evaluation of sampling convergence and adequacy, were identical to those of the molecular analyses.

Alternative phylogenetic positions of *Scaphiophryne* with respect to other microhylids were evaluated using a Shimodaira and Hasegawa (SH) nonparametric likelihood ratio test (49). Two alternative trees, incorporating the basal divergence between *Scaphiophryne* and the remaining Microhylidae and between *Scaphiophryne* and *Paradoxophyla* and the remaining Microhylidae, respectively, were estimated by constrained maximum likelihood (ML) searches under a GTR + G + I model (−lnL = 174,224.89 and −lnL = 174,187.36, respectively) and compared with the unconstrained ML tree (−lnL = 174,174.23) using the SH test implemented in PAUP*.

Posttree analyses. Five MP trees were randomly selected for the parsimony-based estimation of (*i*) ancestral character states for all internal nodes for subsequent morphospace reconstructions, (*ii*) branch-specific amounts of change (morphological branch lengths) for the subsequent inference of rate patterns, and (*iii*) branch-specific apomorphies and their character- and state-specific amounts of change for the subsequent inference of homoplasy patterns per radiation (Fig. S1, 5).

All these analyses were performed using both delayed and accelerated transformation (DELTRAN and ACCTRAN, respectively). Posttree analysis of the Bayesian posterior tree set was limited to the use of the reconstructed branch lengths for the inference of rate patterns. Because results using different trees and optimization methods were very similar, we concentrated additional analyses (morphospace construction, time plots, and rate and homoplasy patterns) on the first selected MP tree using DELTRAN optimization. We also used this tree to infer corresponding divergence time estimates and branch durations.

Divergence Times and Branch Durations. To obtain a temporal framework for anuran larval evolution and estimated branch durations for the inference of evolutionary rates, a phylogenetic timescale was required that included divergences among all taxa represented in our morphological analyses (Fig. S1, 6). We estimated divergence times using two fundamentally different Bayesian relaxed clock methods adapted to multigene datasets implemented in MultiDivtime (50) (available at http://statgen.ncsu.edu/thorne/multidivtime.html) and BEAST 1.4.8 (51). The former method models mutational rate variation across the tree under the assumption of autocorrelation across adjacent branches; the latter samples branch-specific rates from an estimated frequency distribution independent of rate autocorrelation. Homologous sequences of four teleost fishes (*Crassius auratus*, *Danio rerio*, *Oncorhynchus mykiss*, and *Oryzias latipes*) were added to root the tree for the MultiDivtime analyses, and three amniotes (*Homo sapiens*, *Mus musculus*, and *Gallus gallus*) were added to provide additional calibration points for both methods. We excluded the mitochondrial genes, because their very high substitution rates (especially in neobatrachians) (18, 28) posed a risk of mutational saturation, biased branch length estimates, and overestimated divergence times (21). Three nuclear gene fragments (BDNF, c-Myc, and POMCA) were also excluded, because their sampling was concentrated on single anuran clades and they lacked a good coverage of other major lineages. The nine remaining nuclear gene fragments constituted 6,683 bp.

We calibrated the amniote divergences using time intervals suggested by Benton and Donoghue (52): 330.4–312.3 Mya for the split between diapsid and synapsid amniotes (*Gallus* vs. *Homo*) and 100.5–65.5 Mya for the split between primates and rodents (*Homo* vs. *Mus*). Based on a time-calibrated supertree analysis of the lissamphibian fossil record, Marjanovic and Laurin (53) proposed maximum and minimum time constraints for the crown origins of Batrachia (the last common ancestor of frogs and salamanders; 275–250 Mya), Caudata (170–155 Mya), Bombinanura (last common ancestor of Costata and other living anurans; 185–170 Mya), and Xenoanura (last common ancestor of Rhinophrynidae and Pipidae; 175–155 Mya). However, the high incidence of ghost lineages within both Anura and Caudata (53) casts doubt on the applicability of the suggested maxima as hard constraints (i.e., eliminating the possibility that the divergence are older than the suggested maximum) (54). Instead, soft maximum time constraints can be used to specify a low prior probability (but not the impossibility) that a divergence is older than a certain age. Because MultiDivtime only accommodates the use of hard constraints, we ran the program using only minimum time constraints suggested by Marjanovic and Laurin (53) [i.e., >250 Mya for Batrachia (based on the Early Triassic fossil *Triadobatrachus massinoti*) (55), >155 Mya for Caudata (based on the Late Jurassic fossil *Iridotriton hechti*) (56), >170 Mya for Bombinanura (based on the Middle Jurassic *Eodiscoglossus oxoniensis*) (57), and >155 Mya for Xenoanura (based on the Late Jurassic *Rhadinosteus parvus*) (58)]. Instead, BEAST allows the implementation of soft time constraints in the form of prior probability distributions for divergence times. We designed a lognormal prior distribution for each of the four divergences such that (*i*) its zero offset corresponds to the suggested minimum (defining it as a hard constraint), (*ii*) its 95 percentile corresponds to the suggested maximum (a soft constraint specifying a prior probability of 0.05 that the node is older), and (*iii*) its median corresponds to the mean of the hard minimum and soft maximum. Even when they are implemented as soft constraints, the conservative maxima proposed by Marjanovic and Laurin (53) pose the risk of underestimating divergence times. Especially if the molecular data add little information to the Bayesian analyses, the posterior distributions of divergence times will depend almost entirely on the specified priors. The time estimates obtained by BEAST for the batrachian and basal anuran divergences, however, are fairly comparable with those of Multidivtime (Table S1) and previous molecular studies (27, 29, 42), indicating that implementation of the soft maxima had little effect on the posterior distributions estimated by BEAST.

Five additional hard minima were applied in both the MultiDivtime and BEAST analyses based on biogeographic arguments: (*i*) >82 Mya for the split between the north American *Ascaphus* and the New Zealand *Leiopelma* based on geological estimates for the isolation of New Zealand from Antarctica (59); (*ii*) >86 Mya for the split between the south American *Pipa* and the African *Xenopus* based on the youngest age estimates for the separation of both continents (60); (*iii*) >65.5 Mya for the split between the Madagascan *Dyscophus* and Indian/Asian Microhylidae (*Dyscophus* vs. *Kaloula*) corresponding to the Late Cretaceous separation of Madagascar and the Indian subcontinent but incorporating the possibility of intervening land bridges or archipelagoes until the end of the Cretaceous (61–63); (*iv*) >35 Mya for the split between Australian Pelodryadinae and South American Phyllomedusinae (*Litoria* and *Nyctimystes* vs. *Phyllomedusa* and *Agalychnis*) based on geological estimates for the final separation of Australia from

Antarctica; and (*v*) >15.97 Mya for the divergence between North American and Eurasian *Hyla* (*H. cinerea* vs. *H. annectans*) based on the oldest fossils in Europe of Burdigalian (Early Miocene) age (64). The use of paleobiogeographic time constraints based on plate tectonics has recently been criticized (12) based on reports of overseas dispersal in amphibians (65–71). However, without any exception, these reports represent relatively short-distance dispersal events, and convincing evidence for long-distance oceanic dispersal (between continents) in amphibians has not yet been found. We, therefore, argue that long-distance oceanic dispersal is not impossible but at least highly improbable in amphibians, and we prefer to incorporate this improbability by adding paleogeographic time constraints.

MultiDivtime requires the input of priors on the age of the ingroup root (the divergence between amphibians and amniotes). In a previous Multidivtime analysis (27), we set priors for the mean and SD of the ingroup root age (crown group tetrapods) equivalent to 345 ± 20 Mya, without any further constraints on its maximum age. The resulting divergence time estimates for early tetrapod splits (Late Devonian) seemed too old in light of the early tetrapod fossil record. To correct this, *rttm* and *rttmsd* were now set equivalent to 330.4 ± 10 Mya based on the minimum proposed by Benton and Donoghue (52). Additionally, we define 330.4 and 359.2 Mya as minimum and maximum for the age of this node. Together, these priors and time constraints describe one-half of a normal curve, with its modus at 330.4 Mya and its single tail cutoff at 359.2 Mya, forcing the tetrapod crown group to be of Carboniferous age. BEAST does not require a prior on the ingroup root age, but using ref. 52, we set a log-normal prior distribution for the amphibian–amniote split with zero offset at 330.4 Mya and the 95 percentile at 350.1 Mya. An additional hard constraint was set at 359.2 Mya.

For the Multidivtime analyses, DNA substitution branch lengths were estimated for each gene fragment with the program Estbranches using an F84 + G model with parameters estimated by PAUP*. Optimized branch lengths and their variance–covariance matrices were used as input for the program Multidivtime, which calculates 95% credibility intervals for node ages based on relaxed clock model priors and calibration points. The priors for the mean and SD of the ingroup root rate, *rtrate* and *rtratesd*, were both set to 0.1554 (substitutions per site per 100 Myr) based on the median of the substitution path lengths between the ingroup root and each terminal divided by *rttm* (as suggested by the Multidivtime creator). The priors for the mean and SD of the Brownian motion constant v, *brownmean* and *brownsd*, were both set to 0.5. In a previous study, we have shown that changes to these priors have relatively little effect on the posterior divergence time estimates produced by Multidivtime (27). Two independent MCMC chains were run for 1.1 million generations, with a sampling frequency of 1 per 100 generations and a burn-in corresponding to the first 100,000 generations. The .samp output files, containing sampled rates and divergence times, were examined with the program Tracer to check whether sufficiently large effective sampling sizes (>200) were obtained for all divergences and to confirm convergence of the two runs to similar divergence time estimates.

For the BEAST analyses, mutational rate variation across the tree was modeled by sampling branch-specific rates from a log-normal distribution with estimated mean and SD. The underlying DNA substitution process was described using a mixed GTR + G + I model partitioned over the nine gene fragments. To reduce computation time, all GTR + G + I model parameters were fixed to their maximum likelihood values as estimated on the starting tree using PAUP*. In addition, we fixed the tree topology by eliminating the MCMC operators that control branch swapping. BEAST allows the incorporation of a pure birth or birth–death process to model speciation during divergence time analyses. We decided not to use those in our analyses, because previous studies have indicated major clade- and time-dependent variations in net diversification rates in amphibians (27, 42). The assumption of a single net diversification rate (*BminusDRate*) and relative extinction rate (*DoverB*) across the tree would, therefore, entail an oversimplified and biologically unrealistic model of amphibian cladogenesis, and the estimated parameters could be strongly biased by the limited lineage sampling, especially in amniotes and caudates. In other words, the actual ultrametric tree that underlies the taxa included in this study is unlikely to reflect a singular pure birth or birth–death model. To exclude the speciation model from the BEAST analyses, we deleted all MCMC operator commands that specify its model parameters from the BEAST input file. As a result, BEAST will only use the molecular dataset, DNA substitution model, tree, and specified priors on some divergence times to infer posterior divergence times.

Four independent MCMC chains were run for 100 million generations, with a sampling frequency of 1 per 1,000 generations. The log output files containing sampled model parameters and divergence times were examined with Tracer to determine appropriate burn-in intervals and check for sufficiently large effective sampling sizes (>200 when the four runs were combined).

Branch durations were calculated by subtracting (for each branch) the estimated mean divergence time of its terminal node from that of its parental node. Total branch durations for radiations were obtained by summing the durations of all branches included; 95% credibility intervals for total branch durations were obtained under the different relaxed clock models by doing the same subtraction for 10,000 sets of divergence times sampled by MultiDivtime (in the .samp output file) and BEAST and then determining percentiles 2.5 and 97.5.

Reconstruction of Morphospace. The 131 characters of extant anuran tadpoles and DELTRAN-reconstructed ancestors were combined in a larger dataset to estimate a pair-wise distance matrix corrected for missing data (Fig. S1, 7). This matrix was used as input for multidimensional scaling (MDS) performed with Statistica 8 (72), where the distance matrix was treated as a dissimilarity matrix with 131 underlying variables. The minimum number of dimensions required to capture the essential aspects of morphospace was determined by visual inspection of a Scree plot of raw stress values (Fig. S5*A*) and searching the *n*th dimension for which the raw stress change rate was highest (i.e., the dimension that represented the largest descent in stress compared with $n - 1$ dimensions (73). The largest descent was observed when the stress value of a 2D frame was compared with that of a 1D frame. Use of 3D did not drastically change the morphospace patterns observed in a 2D frame (Fig. S5*B*). To evaluate the possibility of biases because of the inclusion of (potentially unrealistic) ancestors, we performed a second MDS analysis using a distance matrix that included only extant tadpoles (Fig. S5*C*).

Estimation of Evolutionary Rates. Time plots of evolutionary change were made by plotting branch-specific amounts of morphological change against corresponding branch durations in a cumulative way from past to present (Fig. S1, 8). As a result, the slope of each branch is proportional to the average evolutionary rate along that branch. The time plots based on DELTRAN optimization of morphological branch lengths are presented in Fig. 2, but branch lengths obtained under ACCTRAN optimization and the Bayesian Mk1 + G model yielded similar plots (Fig. S6). Phylogenetic estimates of amounts of evolutionary change are sensitive to artifacts related to stochastic rate variation and taxon sampling (node density artifacts) (74, 75). To evaluate whether our estimates were affected by such artifacts, we compared the observed amounts of morphological change for each branch with those simulated under a null model of constant (equiprobable) change. We proceeded as follows:

i) We imported the estimated timescale into the program Mesquite 2.5 (76) to simulate the evolution of 65,500 characters, which resulted in 500 replicate datasets of 131 characters. During the simulation, we maintained the same proportions of binary and multistate characters and the same rate variation across characters as in the original dataset.

ii) The 500 datasets were subsequently imported into PAUP* to estimate branch lengths on the chronogram topology under DELTRAN parsimony optimization.

iii) The 500 resulting phylograms were standardized by rescaling to a total tree length of 1.0. The same was done with the empirical DELTRAN-estimated phylogram. This step was required to cancel out the effect of total tree length variation caused by the simulation.

iv) The standardized phylograms were used to obtain (for each branch) a null distribution of branch lengths, reflecting the expected variation under random change. The empirical branch lengths were then individually compared with their corresponding null distributions to determine the probability that they reflect random change across the tree.

Average evolutionary rates per radiation (expressed in number of changes per million years) were calculated by dividing the sum of reconstructed changes over all its branches by its total branch duration derived from the divergence time estimates. Confidence intervals for these rates were based on 500 replicates of character bootstrapping generated with the program *Seqboot* of the Phylip 3.6 software package (77). To incorporate the uncertainty on divergence time estimation, we determined joint 2.5 and 97.5 percentiles on the rates by dividing the 2.5 percentile of the summed morphological branch lengths by the 97.5 percentile of the corresponding branch duration and vice versa.

Analyses of Homoplasy. We examined homoplasy across anuran radiations using the traditional homoplasy index (HI) derived from the consistency index (78) as well as a state-specific homoplasy index (HI_S) (Fig. S1, 9). For each character state change reconstructed on a radiation's branch, HI_S indicates the number of times that it independently occurred elsewhere in the tree. Both indices are likely to be correlated, but HI_S has the advantage over HI that it allows distinction between rare and highly recurrent changes within characters that evolve under highly asymmetric rates. HI values were derived from the credibility interval (CI) values produced per tree branch using the describe trees option in PAUP*. HI_S values were calculated manually based on DELTRAN-optimized character state reconstructions in Mesquite. The distribution of HI and HI_S across all branches of a radiation was visualized using box plots (Fig. 3).

To examine the level of homoplasy shared pair-wise between two radiations or clades, we counted the number of character states that appeared in both of them. Although this provides an absolute estimate of shared homoplasy, it gives little information about the level of significance of the observed homoplasy. For a constant number of possible character states, the expected number of shared homoplastic state changes will increase in function of the total number of state changes in both radiations/clades. In other words, two clades with a high number of state changes will by chance share more homoplasy than two clades with few changes, even when all possible state changes had equal probability. We, therefore, calculated for each pair of radiations/clades the probability of observing the counted number of shared homoplastic state origins h if changes were randomly drawn from a constant set of possible state changes (i.e., if all state changes had equal probability of occurrence). This probability is given by the equation (Eq. **S1**)

$$P(h) = \frac{\binom{s_1}{h} \times \binom{S - s_1}{s_2 - h}}{\binom{S}{s_2}}, \qquad \textbf{[S1]}$$

where S is the total number of states in the dataset ($S = 308$ in our case), s_1 is the number of different state changes observed in radiation/clade 1, and s_2 is the number of different state changes observed in radiation/clade 2. Note that the same probability is obtained when the two radiations/clades (i.e., s_1 and s_2) are exchanged in the equation. Analogously, we calculated the probability $P(e)$ that the observed number of evolving characters e shared between a pair of radiations/pairs reflects the number expected when characters are randomly drawn from a constant set $C = 131$, and the observed numbers of evolving characters in radiations/clades 1 and 2 are c_1 and c_2, respectively (Eq. **S2**):

$$P(e) = \frac{\binom{c_1}{e} \times \binom{C - c_1}{c_2 - e}}{\binom{C}{c_2}}. \qquad \textbf{[S2]}$$

A potential bias on these probability estimations could stem from the possibility that there are actually more possible states (or evolvable characters) than observed in the dataset. However, from Eqs. **S1** and **S2**, it follows that underestimation of S or C results in conservative (less significant) estimates of the inferred probabilities.

1. Haas A (2003) Phylogeny of frogs as inferred from primarily larval characters. *Cladistics* 19:23–89.
2. Orton GI (1957) The bearing of larval evolution on some problems in frog classification. *Syst Zool* 6:79–86.
3. Starrett PH (1973) In *Evolutionary Biology of the Anurans: Contemporary Research on Major Problems*, ed Vial JL (University of Missouri Press, Columbia, MO), pp 251–297.
4. Sokol OM (1975) The phylogeny of anuran larvae: A new look. *Copeia* 1975:1–23.
5. Duellman WE, Trueb L (1992) *Biology of Amphibians* (McGraw-Hill, New York), 2nd Ed.
6. Thompson JD, Gibson TJ, Plewniak F, Jeanmougin F, Higgins DG (1997) The CLUSTAL_X windows interface: Flexible strategies for multiple sequence alignment aided by quality analysis tools. *Nucleic Acids Res* 25:4876–4882.
7. Stamatakis A, Hoover P, Rougemont J (2008) A rapid bootstrap algorithm for the RAxML Web servers. *Syst Biol* 57:758–771.
8. Stamatakis A (2006) RAxML-VI-HPC: Maximum likelihood-based phylogenetic analyses with thousands of taxa and mixed models. *Bioinformatics* 22:2688–2690.
9. Ronquist F, Huelsenbeck JP (2003) MrBayes 3: Bayesian phylogenetic inference under mixed models. *Bioinformatics* 19:1572–1574.
10. Rambaut A, Drummond AJ (2007) *Tracer v1.4*. Available at http://beast.bio.ed.ac.uk/Tracer. Accessed June 2009.
11. Biju SD, Bossuyt F (2003) New frog family from India reveals an ancient biogeographical link with the Seychelles. *Nature* 425:711–714.
12. Blackburn DC, Bickford DP, Diesmos AC, Iskandar DT, Brown RM (2010) An ancient origin for the enigmatic flat-headed frogs (Bombinatoridae: *Barbourula*) from the islands of Southeast Asia. *PLoS One* 5:e12090.
13. Bossuyt F, Brown RM, Hillis DM, Cannatella DC, Milinkovitch MC (2006) Phylogeny and biogeography of a cosmopolitan frog radiation: Late cretaceous diversification resulted in continent-scale endemism in the family ranidae. *Syst Biol* 55:579–594.
14. Darst CR, Cannatella DC (2004) Novel relationships among hyloid frogs inferred from 12S and 16S mitochondrial DNA sequences. *Mol Phylogenet Evol* 31:462–475.
15. Faivovich J, et al. (2005) Systematic review of the frog family Hylidae, with special reference to Hylinae: Phylogenetic analysis and taxonomic revision. *Bull Am Mus Nat Hist* 294:1–240.
16. Frost DR, et al. (2006) The amphibian tree of life. *Bull Am Mus Nat Hist* 297:1–370.
17. García-París M, Buchholz DR, Parra-Olea G (2003) Phylogenetic relationships of Pelobatoidea re-examined using mtDNA. *Mol Phylogenet Evol* 28:12–23.
18. Gissi C, San Mauro D, Pesole G, Zardoya R (2006) Mitochondrial phylogeny of Anura (Amphibia): A case study of congruent phylogenetic reconstruction using amino acid and nucleotide characters. *Gene* 366:228–237.
19. Grant T, et al. (2006) Phylogenetic systematics of dart-poison frogs and their relatives (Anura: Athesphatanura: Dendrobatidae). *Bull Am Mus Nat Hist* 299:184–203.
20. Hoegg S, Vences M, Brinkmann H, Meyer A (2004) Phylogeny and comparative substitution rates of frogs inferred from sequences of three nuclear genes. *Mol Biol Evol* 21:1188–1200.
21. Igawa T, Kurabayashi A, Usuki C, Fujii T, Sumida M (2008) Complete mitochondrial genomes of three neobatrachian anurans: A case study of divergence time estimation using different data and calibration settings. *Gene* 407:116–129.
22. Irisarri I, San Mauro D, Green DM, Zardoya R (2010) The complete mitochondrial genome of the relict frog *Leiopelma archeyi*: Insights into the root of the frog Tree of Life. *Mitochondrial DNA* 21:173–182.

23. Pramuk JB (2006) Phylogeny of South American *Bufo* (Anura: Bufonidae) inferred from combined evidence. *Zool J Linn Soc* 146:407–452.
24. Pramuk JB, Robertson T, Sites JW Jr., Noonan BP (2008) Around the world in 10 million years: Biogeography of the nearly cosmopolitan true toads (Anura: Bufonidae). *Glob Ecol Biogeogr* 17:72–83.
25. Roelants K, Jiang J, Bossuyt F (2004) Endemic ranid (Amphibia: Anura) genera in southern mountain ranges of the Indian subcontinent represent ancient frog lineages: Evidence from molecular data. *Mol Phylogenet Evol* 31:730–740.
26. Roelants K, Bossuyt F (2005) Archaeobatrachian paraphyly and pangaean diversification of crown-group frogs. *Syst Biol* 54:111–126.
27. Roelants K, et al. (2007) Global patterns of diversification in the history of modern amphibians. *Proc Natl Acad Sci USA* 104:887–892.
28. San Mauro D, García-París M, Zardoya R (2004) Phylogenetic relationships of discoglossid frogs (Amphibia:Anura:Discoglossidae) based on complete mitochondrial genomes and nuclear genes. *Gene* 343:357–366.
29. San Mauro D, Vences M, Alcobendas M, Zardoya R, Meyer A (2005) Initial diversification of living amphibians predated the breakup of Pangaea. *Am Nat* 165:590–599.
30. Santos JC, Coloma LA, Cannatella DC (2003) Multiple, recurring origins of aposematism and diet specialization in poison frogs. *Proc Natl Acad Sci USA* 100: 12792–12797.
31. Smith SA, Stephens PR, Wiens JJ (2005) Replicate patterns of species richness, historical biogeography, and phylogeny in Holarctic treefrogs. *Evolution* 59:2433–2450.
32. Smith SA, de Oca AN, Reeder TW, Wiens JJ (2007) A phylogenetic perspective on elevational species richness patterns in Middle American treefrogs: Why so few species in lowland tropical rainforests? *Evolution* 61:1188–1207.
33. Van Bocxlaer I, Roelants K, Biju SD, Nagaraju J, Bossuyt F (2006) Late Cretaceous vicariance in Gondwanan amphibians. *PLoS One* 1:e74.
34. Van Bocxlaer I, Biju SD, Loader SP, Bossuyt F (2009) Toad radiation reveals into-India dispersal as a source of endemism in the Western Ghats-Sri Lanka biodiversity hotspot. *BMC Evol Biol*, 10.1186/1471-2148-9-131.
35. van der Meijden A, Vences M, Meyer A (2004) Novel phylogenetic relationships of the enigmatic brevicipitine and scaphiophrynine toads as revealed by sequences from the nuclear Rag-1 gene. *Proc Biol Sci* 271(Suppl 5):S378–S381.
36. van der Meijden A, Vences M, Hoegg S, Meyer A (2005) A previously unrecognized radiation of ranid frogs in Southern Africa revealed by nuclear and mitochondrial DNA sequences. *Mol Phylogenet Evol* 37:674–685.
37. van der Meijden A, et al. (2007) Nuclear gene phylogeny of narrow-mouthed toads (Family: Microhylidae) and a discussion of competing hypotheses concerning their biogeographical origins. *Mol Phylogenet Evol* 44:1017–1030.
38. Vences M, Kosuch J, Glaw F, Böhme W, Veith M (2003) Molecular phylogeny of hyperoliid treefrogs: Biogeographic origin of Malagasy and Seychellean taxa and re-analysis of familial paraphyly. *J Zoological Syst Evol Res* 41:205–215.
39. Vences M, et al. (2003) Multiple overseas dispersal in amphibians. *Proc Biol Sci* 270: 2435–2442.
40. Wiens JJ, Fetzner JW, Parkinson CL, Reeder TW (2005) Hylid frog phylogeny and sampling strategies for speciose clades. *Syst Biol* 54:778–807.
41. Wiens JJ, Graham CH, Moen DS, Smith SA, Reeder TW (2006) Evolutionary and ecological causes of the latitudinal diversity gradient in hylid frogs: Treefrog trees unearth the roots of high tropical diversity. *Am Nat* 168:579–596.
42. Wiens JJ (2007) Global patterns of diversification and species richness in amphibians. *Am Nat* 170(Suppl 2):S86–S106.
43. Wiens JJ, Sukumaran J, Pyron RA, Brown RM (2009) Evolutionary and biogeographic origins of high tropical diversity in old world frogs (Ranidae). *Evolution* 63:1217–1231.
44. Swofford DL (2002) *PAUP*. Phylogenetic Analysis Using Parsimony (*and Other Methods), Version 4.0b10.* (Sinauer, Sunderland, MA).
45. Springer MS, Teeling EC, Madsen O, Stanhope MJ, de Jong WW (2001) Integrated fossil and molecular data reconstruct bat echolocation. *Proc Natl Acad Sci USA* 98:6241–6246.
46. Gaubert P, Wozencraft WC, Cordeiro-Estrela P, Veron G (2005) Mosaics of convergences and noise in morphological phylogenies: What's in a viverrid-like carnivoran? *Syst Biol* 54:865–894.
47. Lewis PO (2001) A likelihood approach to estimating phylogeny from discrete morphological character data. *Syst Biol* 50:913–925.
48. Yang Z (1996) Among-site rate variation and its impact on phylogenetic analyses. *Trends Ecol Evol* 11:367–372.
49. Shimodaira S, Hasegawa M (1999) Multiple comparisons of log-likelihoods with applications to phylogenetic inference. *Mol Biol Evol* 16:1114–1116.
50. Thorne JL, Kishino H (2002) Divergence time and evolutionary rate estimation with multilocus data. *Syst Biol* 51:689–702.
51. Drummond AJ, Rambaut A (2007) BEAST: Bayesian evolutionary analysis by sampling trees. *BMC Evol Biol* 7:214.
52. Benton MJ, Donoghue PC (2007) Paleontological evidence to date the tree of life. *Mol Biol Evol* 24:26–53.
53. Marjanović D, Laurin M (2007) Fossils, molecules, divergence times, and the origin of lissamphibians. *Syst Biol* 56:369–388.
54. Anderson RJ (2008) Focal review: The origin(s) of modern amphibians. *Evol Biol* 35: 231–247.
55. Rage J-C, Rocek Z (1989) Redescription of *Triadobatrachus massinoti* (Piveteau, 1936) an anuran amphibian from the early Triassic. *Paleontogr Abt A Paleozool Stratigr* 206: 1–16.
56. Evans SE, Lally C, Chure DC, Elder A, Maisano JA (2005) A late Jurassic salamander (Amphibia: Caudata) from the Morrison Formation of North America. *Zool J Linn Soc* 143:599–616.
57. Evans SE, Milner AR, Mussett F (1990) A discoglossid frog from the Middle Jurassic of England. *Palaeontology* 33:299–311.
58. Henrici AC (1998) A new pipoid anuran from the Late Jurassic Morrison Formation at Dinosaur National Monument, Utah. *J Vertebr Paleontol* 18:321–332.
59. Lawver LA, Royer J-Y, Sandwell DT, Scotese CR (1991) *Geological Evolution of Antarctica*, eds Thomson MRA, Crame JA, Thomson JW (Cambridge University Press, Cambridge, UK), pp 533–539.
60. Pittman WC, III, Cande S, LaBrecque J, Pindell J (1993) *Biological Relationships Between Africa and South America*, ed Goldblatt P (Yale University Press, New Haven, CT), pp 15–34.
61. Patriat P, Segoufin J (1988) Reconstruction of the Central Indian Ocean. *Tectonophysics* 155:211–234.
62. Briggs JC (2003) The biogeographic and tectonic history of India. *J Biogeogr* 30: 381–388.
63. Rage J-C (2003) Relationships of the Malagasy fauna during the Late Cretaceous: Northern or southern routes? *Acta Palaeontol Pol* 48:661–662.
64. Rage J-C, Rocek Z (2003) Evolution of anuran assemblages in the Tertiary and Quaternary of Europe, in the context of palaeoclimate and palaeogeography. *Amphib-reptil* 24:133–167.
65. Brown RM, Guttman SI (2002) Phylogenetic systematics of the *Rana signata* complex of Philippine and Bornean stream frogs: Reconsideration of Huxley's modification of Wallace's Line at the Oriental-Australian faunal zone interface. *Biol J Linn Soc Lond* 76:393–461.
66. Evans BJ, et al. (2003) Phylogenetics of fanged frogs: Testing biogeographical hypotheses at the interface of the asian and Australian faunal zones. *Syst Biol* 52: 794–819.
67. Vences M, et al. (2004) Phylogeography of Ptychadena mascareniensis suggests transoceanic dispersal in a widespread African-Malagasy frog lineage. *J Biogeogr* 31: 593–601.
68. Drewes RC, Wilkinson JA (2004) The California Academy of Sciences Gulf of Guinea Expedition (2001) I. The taxonomic status of the genus *Nesionixalus* Perret, 1976 (Anura: Hyperoliidae), treefrogs of São Tomé and Pŕincipe, with comments on the genus *Hyperolius*. *Proc Calif Acad Sci* 55:395–407.
69. Heinicke MP, Duellman WE, Hedges SB (2007) Major Caribbean and Central American frog faunas originated by ancient oceanic dispersal. *Proc Natl Acad Sci USA* 104: 10092–10097.
70. Measey GJ, et al. (2007) Freshwater paths across the ocean: Molecular phylogeny of the frog Ptychadena newtoni gives insights into amphibian colonization of oceanic islands. *J Biogeogr* 34:7–20.
71. Uyeda JC, Drewes RC, Zimkus BM (2007) The California Academy of Sciences Gulf of Guinea Expeditions (2001, 2006) VI. A new species of *Phrynobatrachus* from the Gulf of Guinea Islands and a reanalysis of *Phrynobatrachus dispar* and *P. feae* (Anura: Phrynobatrachidae). *Proc Calif Acad Sci* 58:367–385.
72. Statsoft Inc. (2007) *Statistica Version 8* (Statsoft Inc., Tulsa, OK).
73. Hou J, Jun SR, Zhang C, Kim SH (2005) Global mapping of the protein structure space and application in structure-based inference of protein function. *Proc Natl Acad Sci USA* 102:3651–3656.
74. Bromham L, Woolfit M, Lee MS, Rambaut A (2002) Testing the relationship between morphological and molecular rates of change along phylogenies. *Evolution* 56: 1921–1930.
75. Venditti C, Meade A, Pagel M (2006) Detecting the node-density artifact in phylogeny reconstruction. *Syst Biol* 55:637–643.
76. Maddison WP, Maddison DR (2008) *Mesquite: A Modular System for Evolutionary Analysis, version 2.5.* Available at http://mesquiteproject.org. Accessed December 15, 2008.
77. Felsenstein J (2005) *PHYLIP (Phylogeny Inference Package) Version 3.6.* (Department of Genome Sciences, University of Washington, Seattle).
78. Kluge AG, Farris JS (1969) Quantitative phyletics and the evolution of anurans. *Syst Zool* 18:1–32.

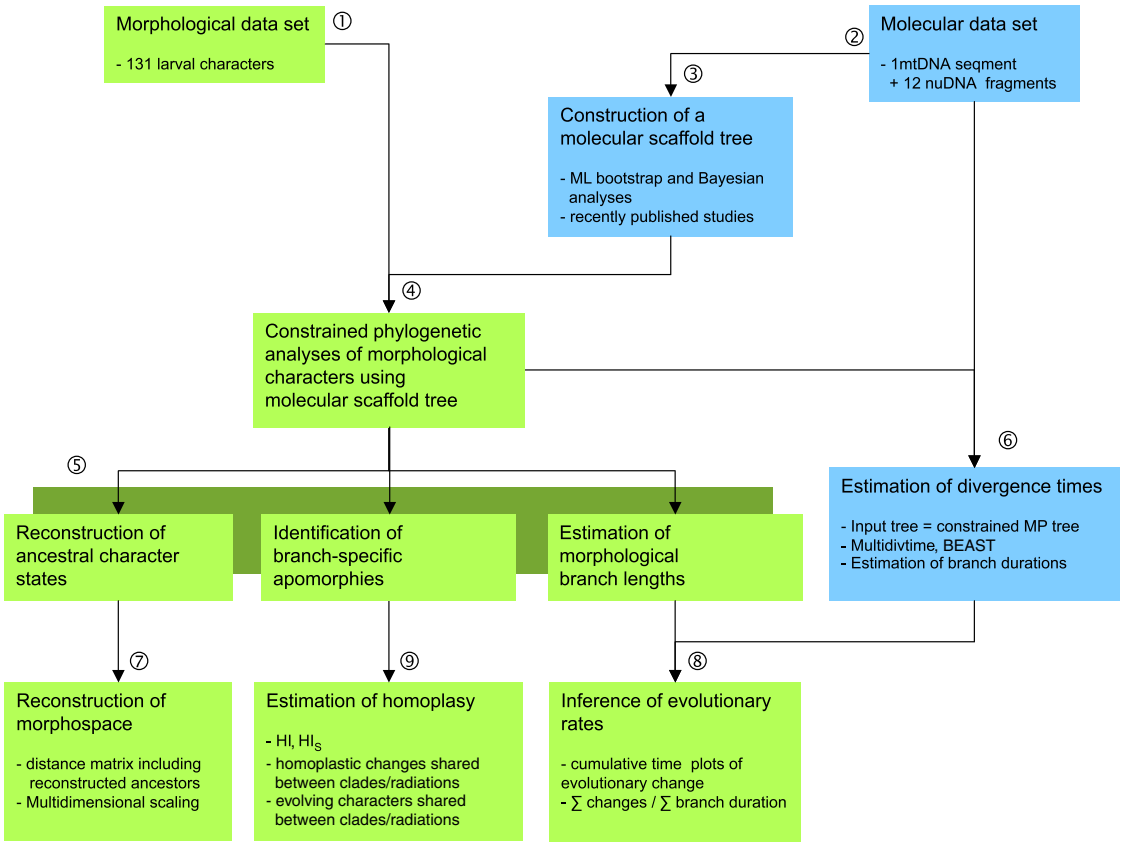

Fig. S1. Flowchart showing the methods used and how they were integrated. Blue boxes indicate the molecular methods. Numbers 1–9 are cross-referenced in *SI Methods*.

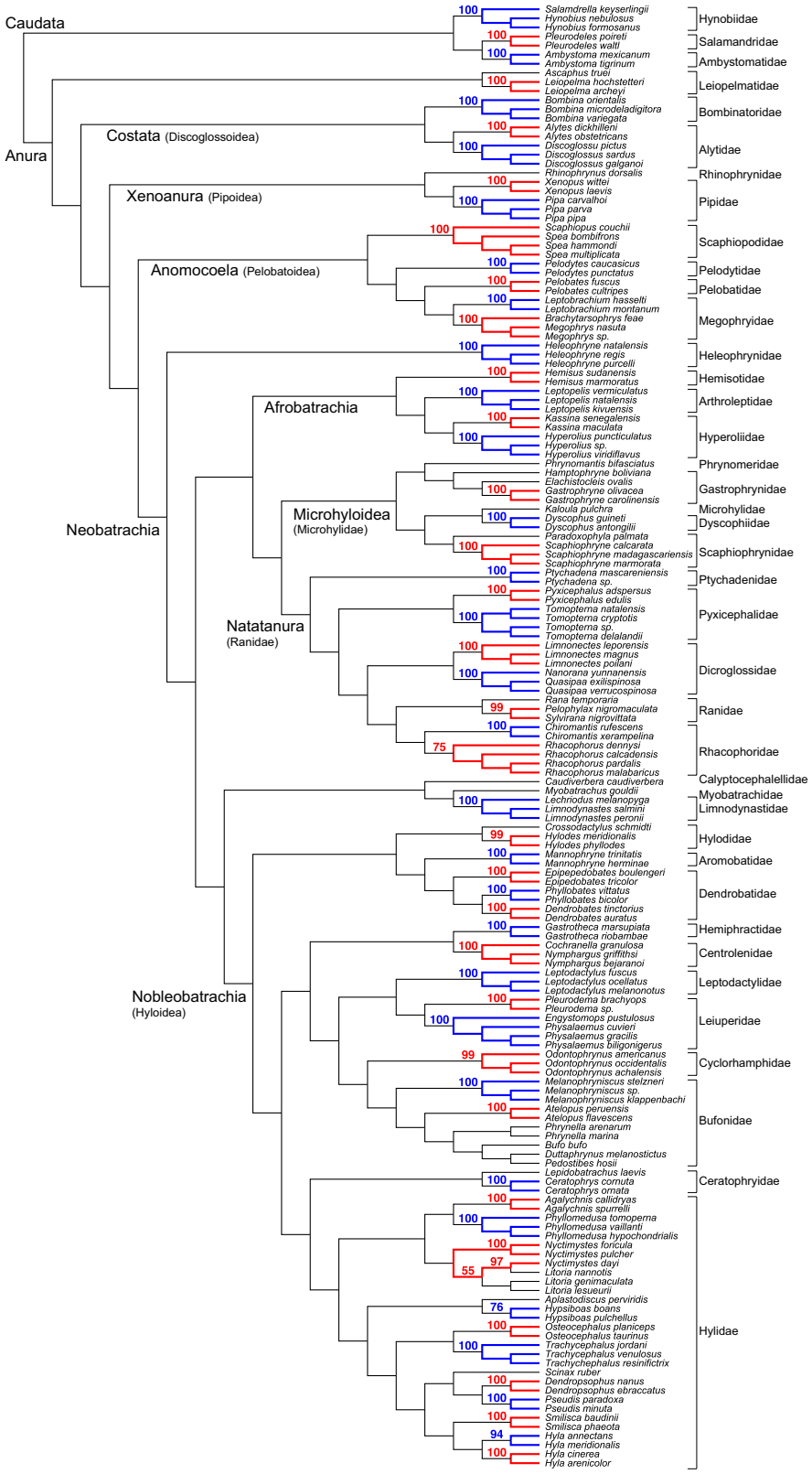

Fig. S2. Consensus tree obtained by 500 replicates of RBS bootstrapping with RAxML using a partitioned GTR model corrected for among-site rate heterogeneity by implementing 25 discrete rate categories (GTR + CAT). Close relationships among most congeneric and confamilial relationships (red and blue branches) are corroborated by high bootstrap support values, justifying the combination of their complementary sequences into single chimeric taxa.

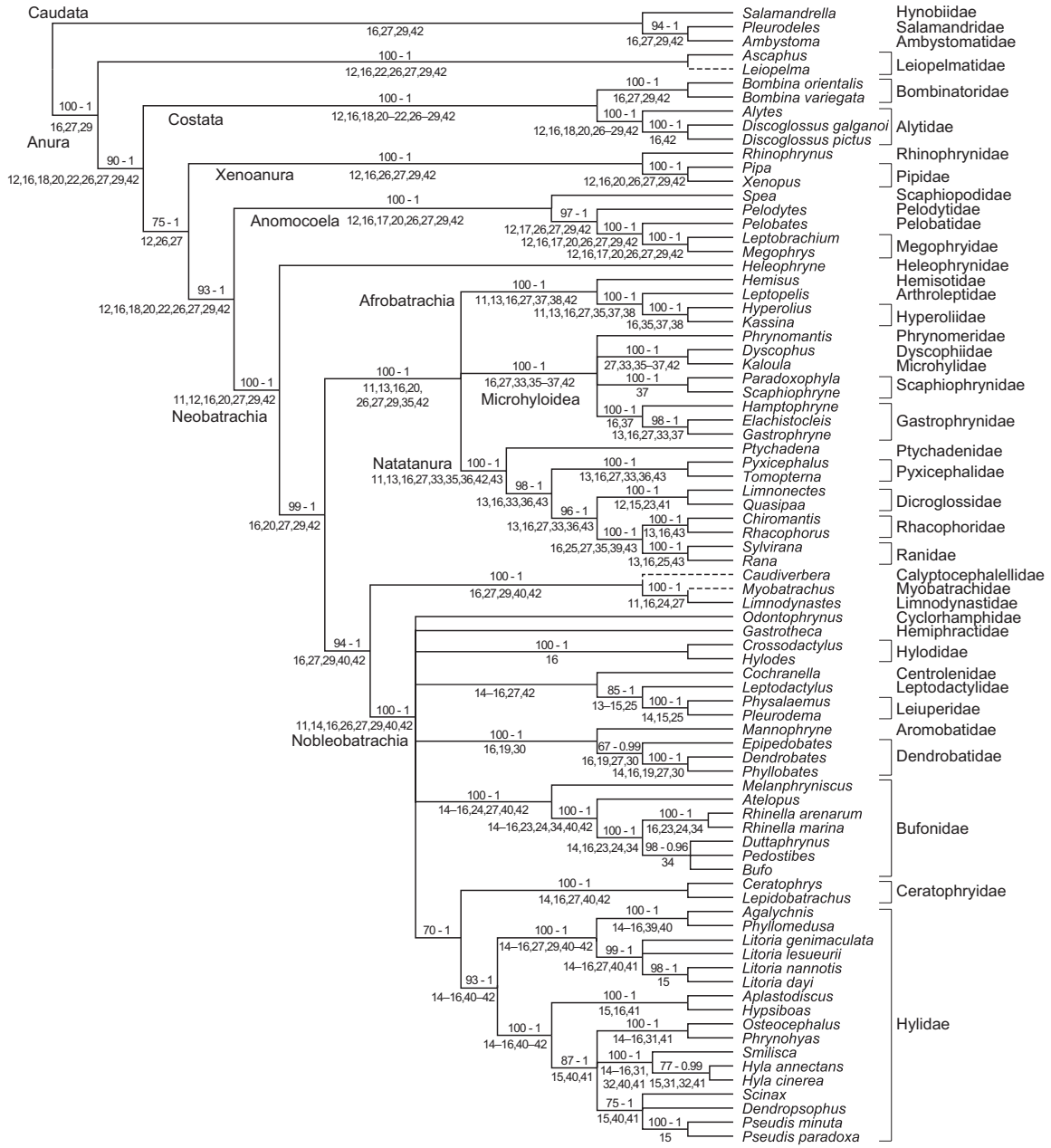

Fig. S3. Molecular scaffold tree used to constrain the morphological analyses. Values above branches are SBS bootstrap percentages (to the left) and Bayesian posterior probabilities (to the right), both estimated under a partitioned GTR + G + I model of DNA substitution. Numbers below branches indicate previous molecular studies supporting the same relationship, and they correspond to references in *SI Methods*.

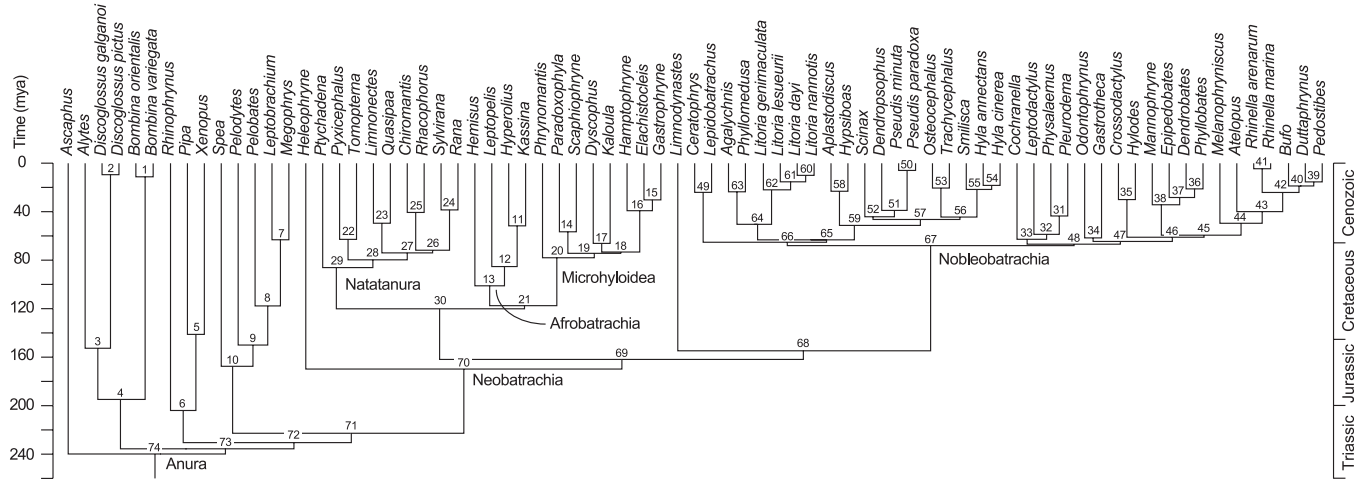

Fig. S4. Phylogenetic timescale for Anura showing mean divergence time estimates as inferred by Multidivtime. Node numbers are cross-referenced in Table S1, listing mean estimates and 95% CI intervals produced by the Multidivtime and BEAST analyses.

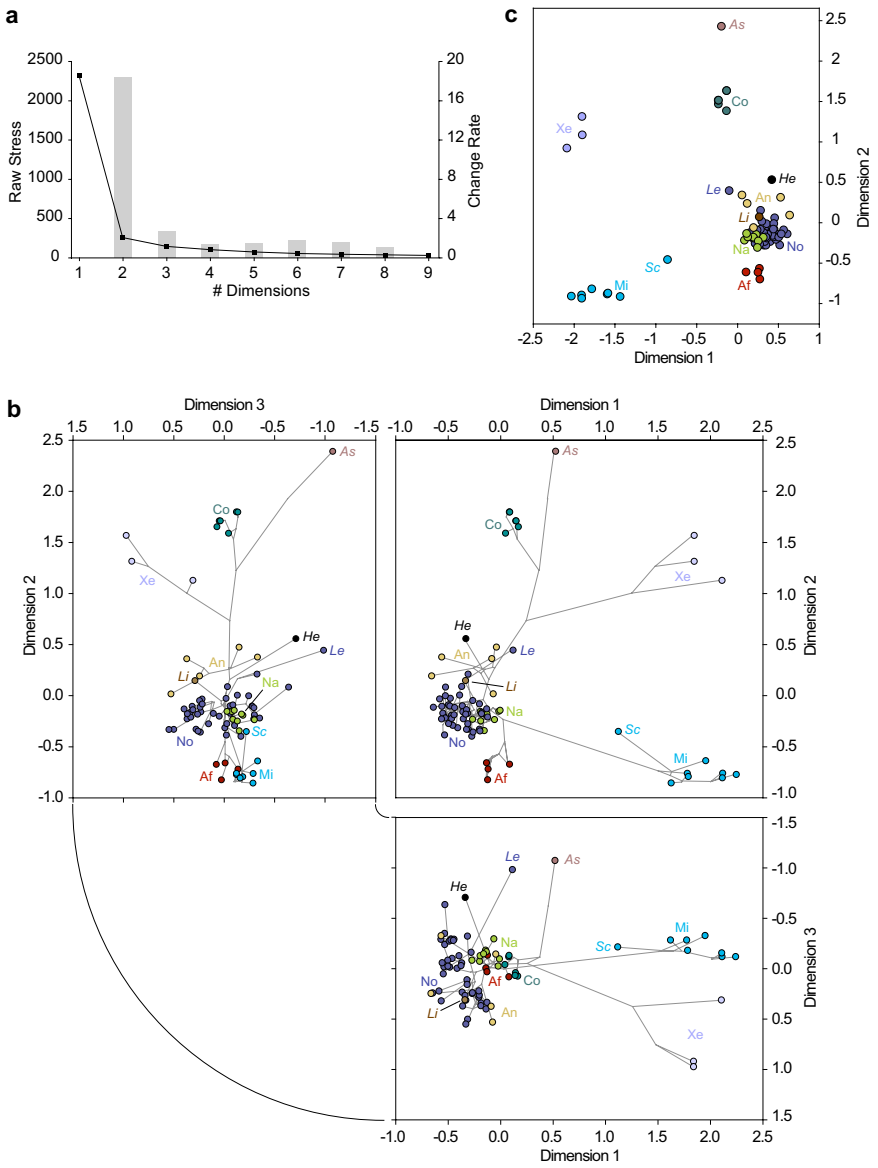

Fig. S5. Morphospace visualization using multidimensional scaling. (*A*) Scree plot of raw stress values (left axis; line plot) used to determine the minimum number of necessary dimensions to capture the essential features of larval morphospace. Raw stress change rates comparing descents of raw stress for successive dimension additions are indicated by the bar diagram (right axis). (*B*) 3D representation of larval morphospace showing a very similar distribution of extant and reconstructed ancestral tadpoles to a 2D frame. (*C*) 2D representation of larval morphospace based on a distance matrix that includes only extant tadpoles (reconstructed ancestors being excluded). A, basal anuran radiation; Af, Afrobatrachia; An, Anomocoela; *As*, *Ascaphus*; Co, Costata; *He*, *Heleophryne*; Le, *Lepidobatrachus*; *Li*, *Limnodynastes*; Mi, Microhyloidea; N, basal neobatrachian radiation; Na, Natatanura; No, Nobleobatrachia; *Sc*, *Scaphiophryne*; Xe, Xenoanura.

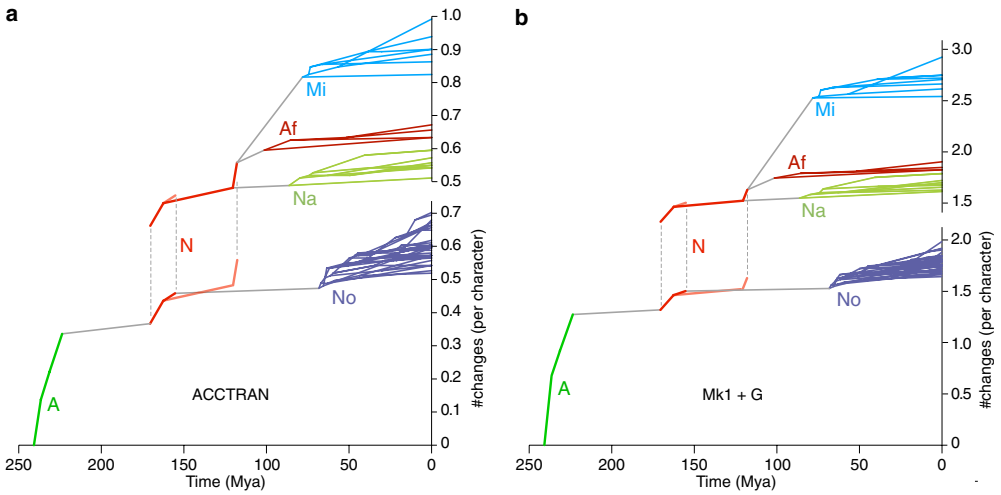

Fig. S6. Cumulative time plots of evolutionary change obtained under ACCTRAN optimization (*A*) and a Bayesian Mk1 + G model of discrete character change (*B*). The slope of each branch is proportional to its average rate of morphological change. A, basal anuran radiation; Af, Afrobatrachia; Mi, Microhyloidea; N, basal neobatrachian radiation; Na, Natatanura; No, Nobleobatrachia.

Table S1. Molecular divergence time estimates obtained by two different Bayesian relaxed clock models

		Correlated model (MultiDivitime)				Uncorrelated log-normal model (BEAST)			
				95% CI				95% CI	
Node*	Clade	Mean (Mya)	SD	2.5%	97.5%	Mean (Mya)	SD	2.5%	97.5%
1		11.2	3.1	6.3	18.3	6.5	0.4	2.7	11.1
2		9.5	4.5	2.0	19.5	7.2	0.3	2.5	12.8
3	Discoglossidae	153.3	10.2	133.6	173.4	115.5	7.4	71.1	157.7
4	Costata	195.7	9.8	176.3	215.4	163.2	5.9	124.0	201.0
5	Pipidae	141.8	9.9	122.8	161.3	114.2	3.5	86.1	137.5
6	Xenoanura	204.8	9.3	187.0	223.2	167.0	5.4	158.7	177.3
7	Megophryidae	63.4	7.6	49.4	79.9	55.6	2.6	36.8	76.3
8		118.2	9.6	99.9	136.7	105.1	3.9	79.9	130.3
9		150.6	10.2	132.3	170.6	134.0	4.6	107.6	160.4
10	Anomocoela	168.2	9.9	149.4	187.8	152.3	5.0	126.5	179.3
11		51.8	5.8	40.7	63.5	46.6	2.1	29.2	65.8
12		85.6	5.1	76.3	96.0	77.6	2.6	58.5	97.2
13	Afrobatrachia	101.5	5.2	91.8	112.0	98.4	2.9	79.7	117.2
14		56.8	3.6	49.7	63.9	58.8	2.1	39.6	76.2
15		30.3	2.8	25.1	35.8	33.2	1.9	20.2	47.5
16		39.3	3.3	33.2	46.1	45.1	2.0	30.3	59.6
17		66.4	0.9	65.5	68.6	69.0	0.9	65.0	76.3
18		73.5	2.0	69.8	77.7	79.6	1.6	71.0	89.6
19		74.6	2.1	70.8	79.1	80.7	1.6	71.9	90.7
20	Microhyloidea	78.3	2.6	73.3	83.5	86.3	1.8	76.1	97.7
21		118.0	4.8	108.8	127.4	118.9	3.0	103.9	134.4
22		63.1	4.7	54.2	72.1	59.0	3.4	39.9	79.2
23		49.7	4.6	40.8	58.5	49.3	3.1	28.6	70.5
24		38.6	4.9	29.6	48.3	35.8	2.2	18.3	54.1
25		40.7	5.9	29.8	52.8	37.0	2.2	21.3	54.3
26		72.0	4.8	62.6	81.7	69.4	3.4	52.3	86.9
27		74.2	4.7	65.4	83.5	75.0	3.5	57.9	92.7
28		80.0	4.8	71.0	89.7	80.9	3.5	63.6	99.1
29	Natatanura	86.4	4.9	76.9	96.3	89.3	3.6	70.5	108.5
30	Ranoides	120.6	4.9	110.9	130.4	125.7	3.2	110.2	142.3
31		43.7	4.3	35.9	52.8	52.1	2.7	34.3	69.9
32		58.9	4.8	50.3	68.8	75.3	3.6	59.7	91.7
33		63.0	4.8	54.0	73.2	85.6	4.1	71.1	101.2
34		61.8	5.0	52.4	72.3	81.2	3.9	65.5	97.6
35		30.1	4.7	21.2	39.8	37.3	2.1	19.0	56.7
36		21.2	2.8	16.3	27.4	27.4	1.9	15.8	40.3
37		28.4	3.3	22.4	35.2	38.7	2.3	25.4	52.9
38		34.4	4.3	26.4	42.9	45.6	2.4	30.6	61.2
39		15.4	2.5	10.9	20.7	18.8	1.2	10.6	27.9
40		18.8	3.2	13.1	25.3	21.0	1.2	12.4	30.5
41		4.5	1.8	1.5	8.3	6.1	2.5	2.3	10.6
42		24.2	3.7	17.1	31.8	31.3	1.7	20.7	42.7
43		40.1	4.5	31.4	49.3	50.1	2.5	36.3	64.8
44	Bufonidae	49.7	4.5	41.3	59.0	63.7	3.1	49.0	78.9
45		59.6	4.8	50.3	69.3	79.5	3.8	65.6	94.4
46		61.3	4.9	52.0	71.3	82.5	3.9	68.2	97.6
47		64.8	4.8	55.7	74.7	85.6	4.0	71.4	100.9
48		67.0	4.8	58.3	77.3	87.9	4.1	73.4	103.2
49		24.1	3.3	18.1	31.1	19.3	1.6	8.7	32.2
50		5.9	2.6	1.3	11.8	11.1	4.6	3.4	20.1
51		39.1	4.6	30.9	48.4	48.9	2.1	35.6	62.5
52		44.3	4.2	36.5	52.6	56.3	2.4	43.5	69.5
53		20.5	3.3	14.5	27.5	27.7	1.4	13.7	42.9
54		18.3	1.7	16.1	22.4	23.7	1.3	16.0	32.7
55		21.7	2.2	17.9	26.2	29.9	1.5	20.5	40.2
56		44.6	3.8	37.8	52.3	56.7	2.4	44.5	69.3
57		46.6	4.0	39.8	54.7	60.6	2.6	48.6	73.6
58		23.2	4.0	15.8	30.9	31.7	1.6	17.1	47.4
59	Hylinae	51.5	4.6	43.3	61.3	67.9	2.9	54.9	81.9

Table S1. Cont.

		Correlated model (MultiDivitime)				Uncorrelated log-normal model (BEAST)			
				95% CI				95% CI	
Node*	Clade	Mean (Mya)	SD	2.5%	97.5%	Mean (Mya)	SD	2.5%	97.5%
60		10.0	4.2	2.2	19.1	13.9	6.0	6.5	22.5
61		15.4	4.5	7.4	25.2	23.1	1.1	12.7	34.2
62		22.0	5.2	12.8	33.6	24.7	1.3	14.0	36.5
63		23.6	3.6	17.5	31.1	29.6	1.7	16.3	44.6
64		50.6	4.5	42.6	60.1	59.7	2.5	42.0	77.8
65	Hylidae	63.4	4.7	54.9	73.3	81.5	3.7	67.3	96.2
66		65.4	4.7	56.6	75.0	88.2	4.1	73.7	103.5
67	Nobleobatrachia	68.2	4.8	59.6	78.0	90.9	4.3	76.3	106.6
68		155.4	7.2	141.0	169.6	145.6	4.9	126.1	166.5
69		162.5	6.9	149.3	175.8	157.5	5.1	138.5	177.8
70	Neobatrachia	170.5	7.1	156.8	184.9	166.4	5.3	146.3	187.4
71		223.7	8.7	206.5	241.3	195.9	5.7	173.3	219.3
72		231.4	8.7	215.0	248.9	206.5	6.0	182.9	230.4
73	Bombinanura	236.6	8.8	219.8	254.6	213.1	6.1	188.7	238.0
74	Anura	240.9	8.8	224.3	259.2	221.7	6.3	196.3	248.1
74	Caudata	225.9	13.5	198.0	250.9	163.2	2.1	157.7	170.3
74	Batrachia	333.3	6.6	319.7	345.4	306.7	3.8	277.3	336.9
74	Tetrapoda	347.5	2.0	342.9	350.0	345.6	8.5	335.7	357.2

CI, credibility interval; Mya, million years ago.
*Node numbers are cross-referenced in Fig. S4.

Other Supporting Information Files

Dataset S1 (XLS)